Supplementary Material

Biomass burning aerosol over the Amazon: analysis of aircraft, surface and satellite observations using a global aerosol model

Carly L. Reddington[1], William T. Morgan[2], Eoghan Darbyshire[2], Joel Brito[3,4], Hugh Coe[2], Paulo Artaxo[3], John Marsham[1], Dominick V. Spracklen[1]

[1]School of Earth and Environment, University of Leeds, Leeds, UK.

[2]Centre of Atmospheric Sciences, School of Earth and Environmental Science, University of Manchester, Manchester, UK.

[3]Physics Institute, University of São Paulo, São Paulo, Brazil.

[4]Now at: Laboratoire de Météorologie Physique, Université Clermont Auvergne, Aubière, France.

Correspondence to: C. L. Reddington (c.l.s.reddington@leeds.ac.uk)

S1. Calculation of aerosol water uptake for simulated aerosol optical depth

S1.1 Description of the online water uptake calculation

In GLOMAP, the water uptake for each soluble aerosol component is calculated online according to Zdanovskii-Stokes-Robinson (ZSR) theory, which estimates the liquid water content as a function of solute molarity (Stokes and Robinson, 1966). For POM in the soluble modes, we assigned an hygroscopicity consistent with a water uptake per mole at 65% of that of SO_4 (Mann et al., 2010). This is likely to be an upper estimate of aerosol hygroscopicity as discussed in Reddington et al. (2016). In the calculation of AOD, we used the resulting hourly mean aerosol wet radii and refractive indices to calculate the hourly aerosol extinction.

S1.2 Description of the offline κ-Köhler water uptake calculation

To calculate the water uptake "offline" we used the κ-Köhler scheme, based upon the Köhler equation with a single parameter, *κ*, defining the water uptake for different chemical species (Petters and Kreidenweis, 2007). The species-dependent hygroscopiticy parameter, *κ*, is defined through its effect upon the water activity of the solution as follows:

$$\frac{1}{a_w} = 1 + \kappa \frac{V_s}{V_w},$$

where *Vs* is the volume of the dry aerosol and *Vw* is the volume of water. For the SO_4 and sea spray components in the model we used the mean values of κ for ammonium sulphate and sodium chloride for subsaturated air masses (0.53 and 1.12, respectively) from Petters and Kreidenweis (2007). BC is considered entirely hydrophobic in this model when using this scheme. We assume a κ value for POM (0.1) based upon aerosol samples collected during the 2008 Amazonian Aerosol Characterization Experiment (AMAZE-08) (Gunthe et al., 2009).

Using Köhler theory and the above equation, the relationship between the relative humidity and the growth of the aerosol can be defined as follows (see Petters and Kreidenweis (2007) for derivation):

$$S(D) = \frac{D^3 - D_d^3}{D^3 - D_d^3(1-\kappa)} \exp\left(\frac{4\sigma_{s/a} M_w}{RT\rho_w D}\right),$$

where S is the saturation ratio, D_d is the dry diameter, D is the wet diameter, κ is the hygroscopic parameter specific to the solute, $\sigma_{s/a}$ is the surface tension of the droplet, R is the universal gas constant, T is the temperature and M_w and ρ_w are the molecular mass and density of water, respectively. In the model this equation is solved iteratively by incrementing D until the saturation ratio is equal to the ambient relative humidity. The growth factor and volume of water can be determined from this and used to calculate the refractive index of the wetted aerosol.

Supplementary Table

#	BC	POM	Description	Reference	Difference from control	NMBF
1	1.750 – 0.442286*i* (λ=542 nm)	1.500 – 0.00*i* (all λ)	Control simulation	Bellouin et al., 2011	-	WP1: -1.48 WP2: -1.37 E: -1.44
2	1.54 – 0.025*i* (λ=550 nm)	1.54 – 0.025*i* (λ=550 nm)	Calculated for young smoke aerosol over southern Africa.	Haywood et al., 2003	W: +3.2% E: +1.3%	WP1: -1.40 WP2: -1.30 E: -1.41
3	1.51 – 0.024*i* (λ=440 nm)	1.51 – 0.024*i* (λ=440 nm)	Retrieved by AERONET station, Ndola in Zambia, located close to smoke sources (Sep 2000 mean)	Matichuk et al., 2007	W: -0.9% E: -2.9%	WP1: -1.51 WP2: -1.39 E: -1.51
4	1.52 – 0.019*i* (λ=440 nm)	1.52 – 0.019*i* (λ=440 nm)	Retrieved by AERONET station, Ndola in Zambia (16 Sep 2000)	Matichuk et al., 2007	W: 0.0% E: -2.2%	WP1: -1.49 WP2: -1.37 E: -1.50
5	1.50 – 0.02*i* (λ=440 nm)	1.50 – 0.02*i* (λ=440 nm)	Retrieved by AERONET station, Jaru Reserve in Brazil (20 Sep 2002)	Matichuk et al., 2008	W: -2.6% E: -4.8%	WP1: -1.56 WP2: -1.43 E: -1.56
6	1.85 – 0.71*i* (λ=550 nm)	[set to 1.500 – 0.000*i*]	Mid-range value for refractive indices for light absorbing carbon	Bond and Bergstrom, 2006	W: +2.2% E: +3.9%	WP1: -1.42 WP2: -1.32 E: -1.36
7	1.95 – 0.79*i* (λ=550 nm)	[set to 1.500 – 0.000*i*]	Upper limit of refractive indices for light absorbing carbon	Bond and Bergstrom, 2006	W: +3.4% E: +5.8%	WP1: -1.39 WP2: -1.29 E: -1.31

Table S1. Range of refractive indices applied to explore the sensitivity of simulated aerosol optical depth (AOD) to assumptions about the aerosol optical properties (Sect. 3.5). Refractive indices were assumed for the BC and POM model components to calculate AOD at a wavelength (λ) of 550 nm (AOD550) to compare with satellite-retrieved (MODIS) AOD550 during the SAMBBA campaign. The mean difference from the control AOD and the normalised mean bias (NMBF) values between model and MODIS AOD550 are given for the eastern (E) and western (W) Amazon regions (shown in Fig. 2 and Fig. S1).

Supplementary figures

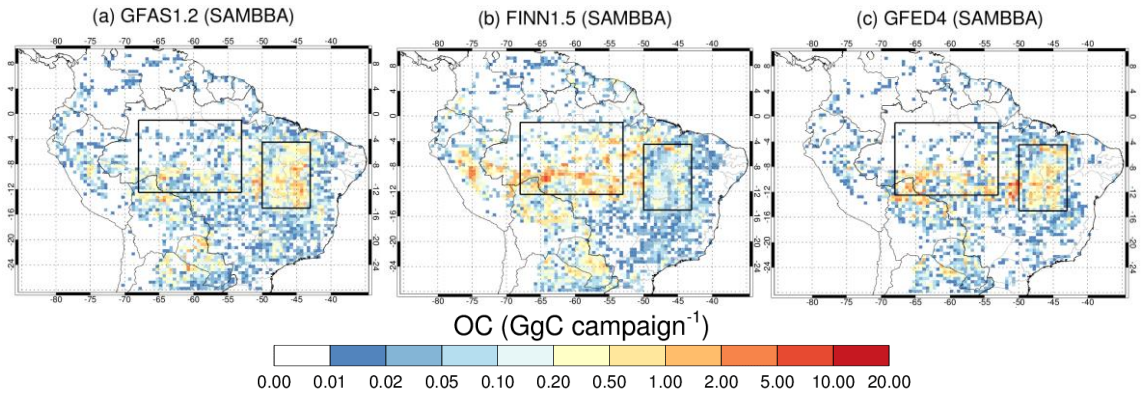

Figure S1. Estimated total organic carbon (OC) aerosol emissions from fire shown for the SAMBBA field campaign (13 September to 3 October 2012). Emissions are shown for **(a)** GFAS version 1.2, **(b)** FINN version 1.5 and **(c)** GFED version 4.1s. The eastern (43-50°W, 4.5-15°S) and western (53-68°W, 1-12.5°S) domains are shown with black boxes.

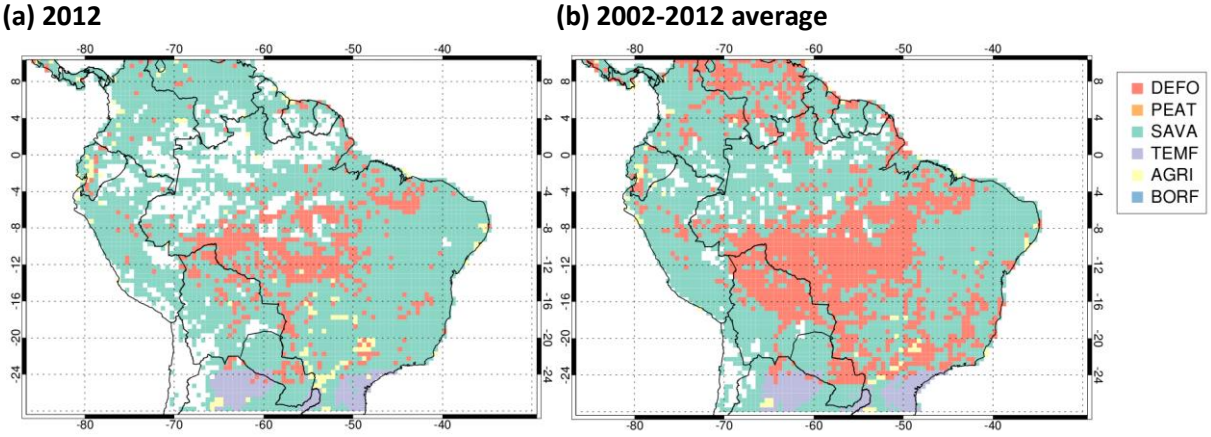

Figure S2. Spatial distribution of the dominant fire types for fire emissions of OC in the Amazon region for **(a)** 2012 and **(b)** 2002-2012. Data is from GFED4 (van der Werf et al., 2010; 2017) re-gridded to 0.5° x 0.5° resolution to be consistent with Fig. 1. Fires are characterised into six types: deforestation and degradation fires (DEFO); peatland fires (PEAT); savanna, grassland, and shrubland fires (SAVA); temperate forest fires (TEMF); agricultural waste burning (AGRI); and boreal forest fires (BORF). The dominant fire type was derived by calculating the maximum GFED4 OC emissions flux for each fire type in each 0.5°x0.5° grid cell over the periods 2002-2012 and 2012.

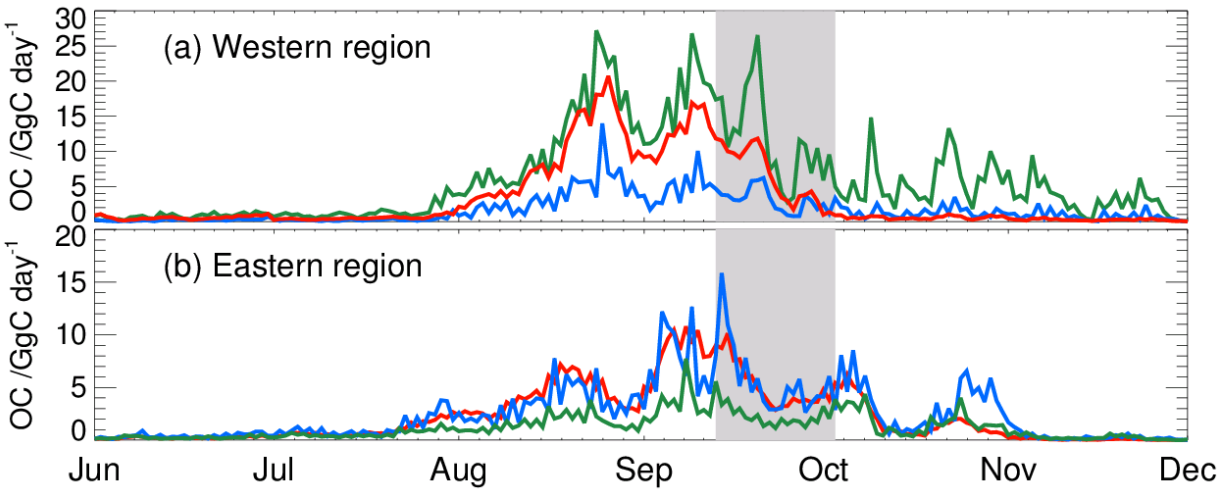

Figure S3. Total daily organic carbon (OC) aerosol emissions from fire for June – November 2012 over **(a)** the western Amazon (53-68°W, 1-12.5°S) and **(b)** the eastern Amazon (43-50°W, 4.5-15°S). Emissions are shown for GFAS version 1.2 (blue), FINN version 1.5 (green) and GFED version 4.1s (red). The SAMBBA campaign period (13 September – 3 October 2012) is shown in grey.

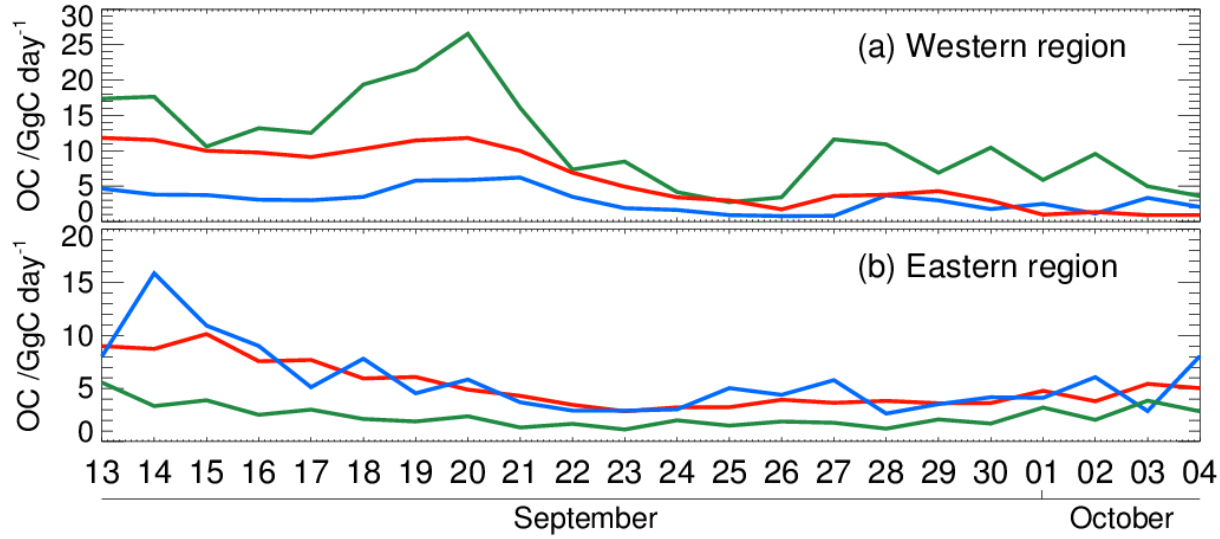

Figure S4. Total daily organic carbon (OC) aerosol emissions from fire for the SAMBBA campaign (13 September – 3 October 2012) over **(a)** the western Amazon (53-68°W, 1-12.5°S) and **(b)** the eastern Amazon (43-50°W, 4.5-15°S). Emissions are shown for GFAS version 1.2 (blue), FINN version 1.5 (green) and GFED version 4.1s (red).

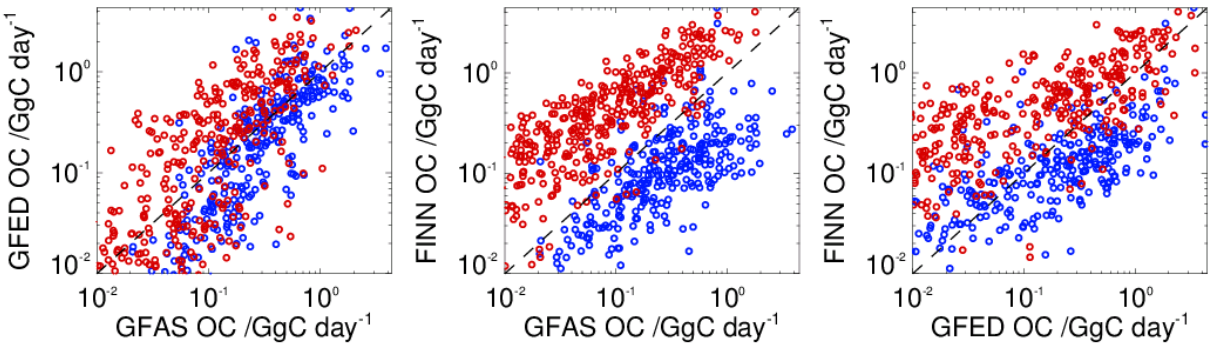

Figure S5. Total daily organic carbon (OC) aerosol emissions from fire in every 0.5°x0.5° grid cell the western Amazon (53-68°W, 1-12.5°S) (red) and the eastern Amazon (43-50°W, 4.5-15°S) (blue), during the SAMBBA campaign (13 September – 3 October 2012). Emissions are shown for GFAS version 1.2, FINN version 1.5 and GFED version 4.1s.

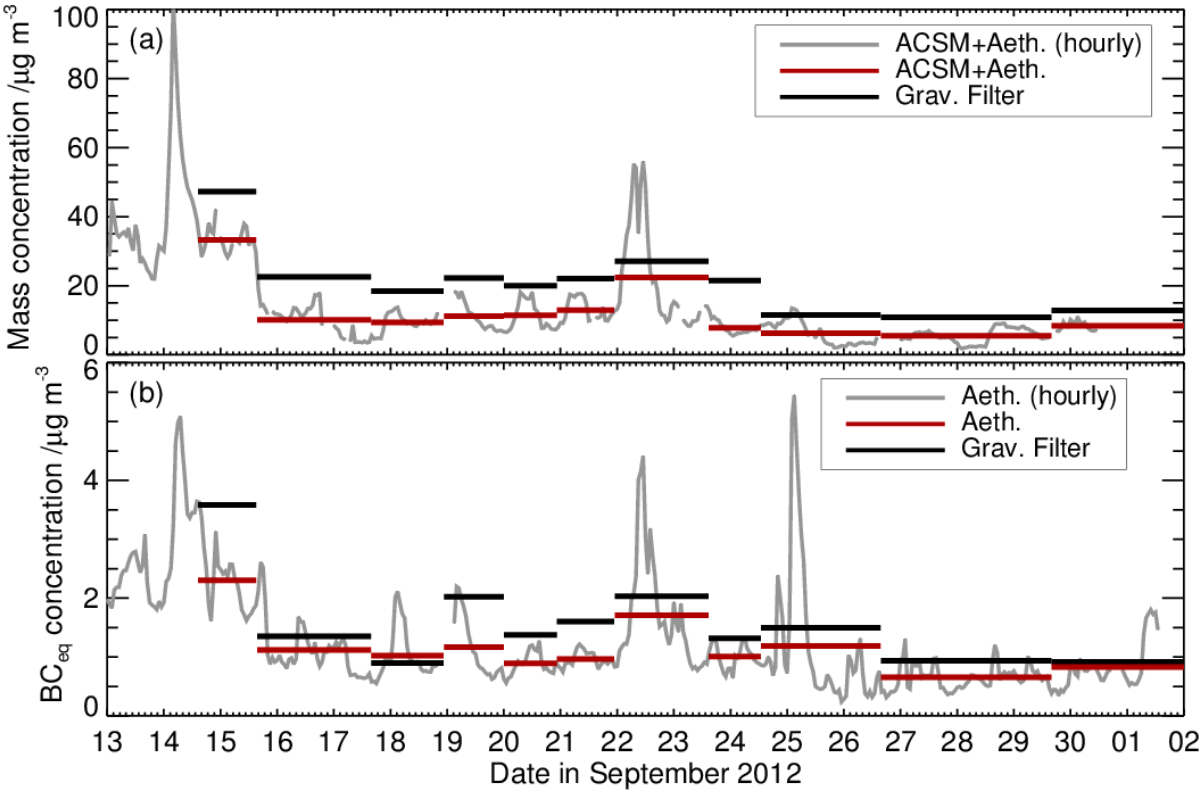

Figure S6. (a) Total aerosol mass concentration measured using gravimetric filter analysis ("Grav. Filter"; for aerosol < 2.5 µm in diameter) and calculated as mass measured by the ACSM plus equivalent black carbon (BC_{eq}) measured by the aethelomter ("ACSM+Aeth."; for aerosol in the 75 - 650 nm diameter range). **(b)** BC_{eq} measured using gravimetric filter analysis ("Grav. Filter"; for aerosol < 2.5 µm in diameter) and the aethelomter ("Aeth."). The ACSM and aethelomter hourly data were averaged over the measurement duration of the gravimetric filter samples.

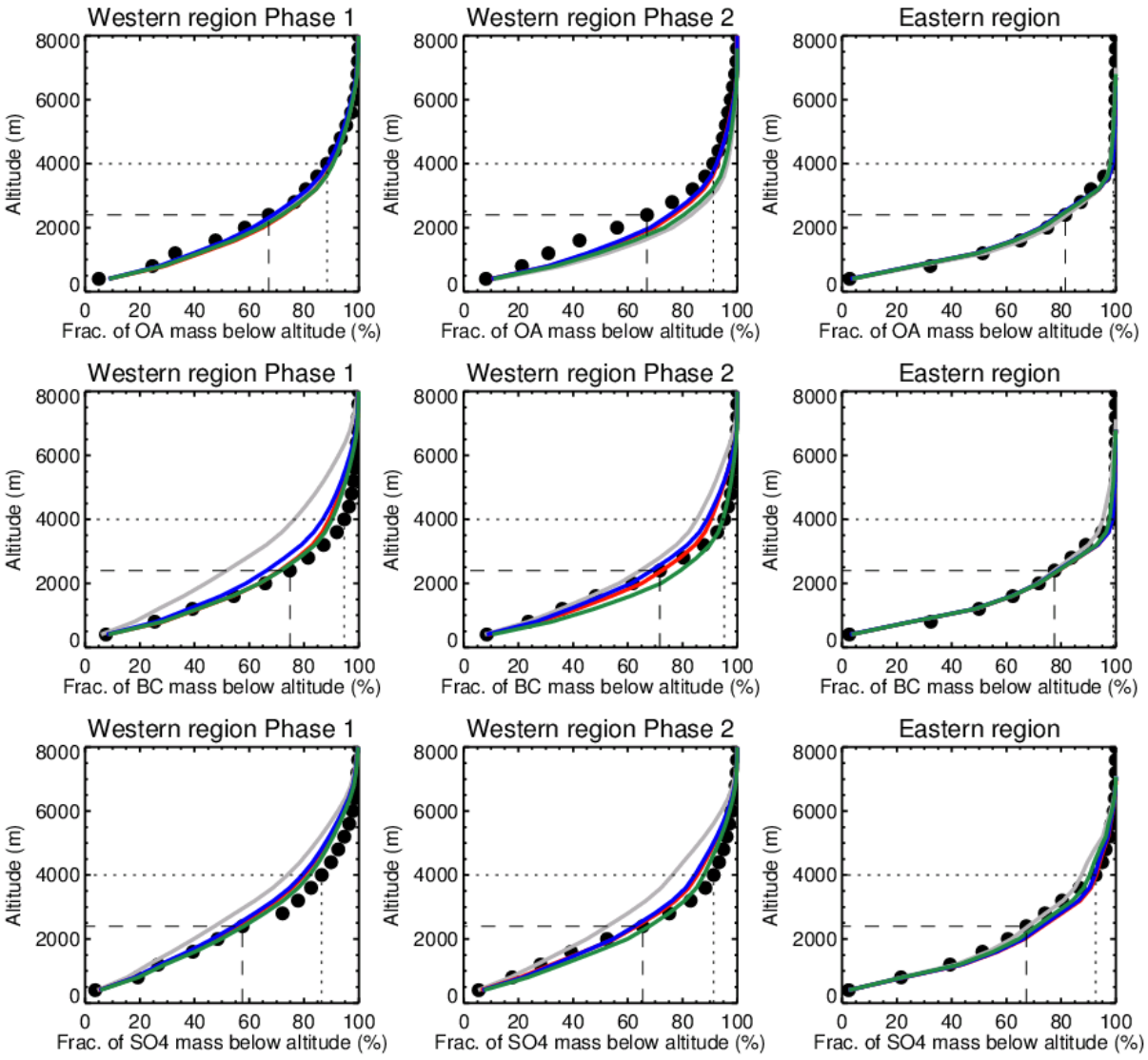

Figure S7. Mean vertical profiles of observed and simulated fraction of aerosol mass column for organic aerosol (OA; top panel), black carbon (BC; middle panel) and sulfate (SO4; bottom panel) during the SAMBBA aircraft campaign, sectioned into 400 m altitude bins. Observations are shown by the black data points; simulated concentrations are shown for the model with FINN1.5 (green), GFAS1.2 (blue), GFED4 (red) emissions and with no biomass burning emissions (grey). The simulated data (linearly interpolated to the flight track of the aircraft) and the observations are split into western and eastern regions of the Amazon (Fig. 2 and Fig. S1) and by time (Phase 1: 13/09/2012 – 22/09/2012, Phase 2: 23/09/2012 - 03/10/2012) for the western region. Observations when the aircraft was specifically targeting smoke plumes have been removed from the analysis. The dashed and dotted lines indicate the fraction of observed aerosol mass below 2.4 km and 4 km altitude, respectively.

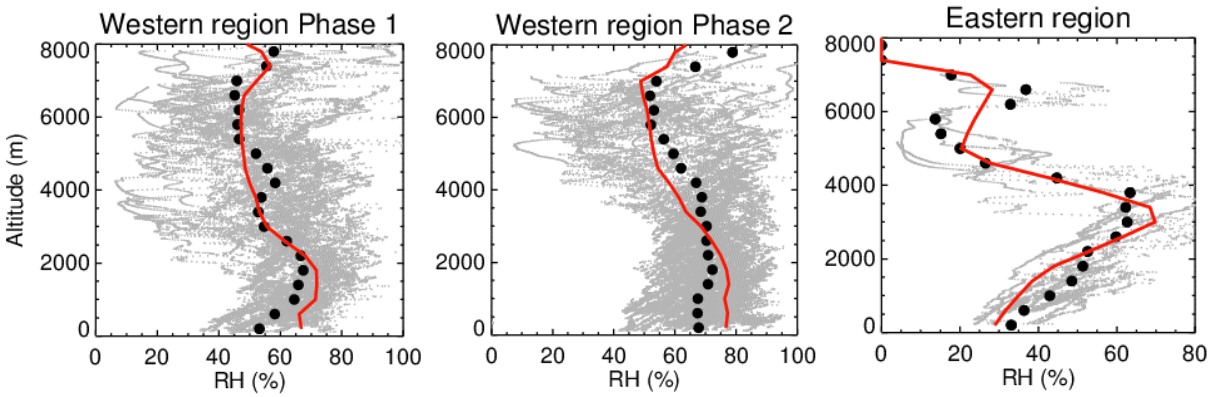

Figure S8. Mean observed and simulated vertical profiles of relative humidity (RH) during the SAMBBA aircraft campaign, sectioned into 400 m altitude bins. Observed RH values are shown by the grey data points; campaign-mean observed RH values are shown by the black data points; campaign-mean GLOMAP RH values are shown by the red line. GLOMAP RH fields are from six-hourly ECMWF ERA-Interim reanalysis data, interpolated onto the model time-step. The GLOMAP data (linearly interpolated to the flight track of the aircraft) and the observations are split into western and eastern regions of the Amazon (Fig. 2 and Fig. S1) and by time (Phase 1: 13/09/2012 – 22/09/2012, Phase 2: 23/09/2012 - 03/10/2012) for the western region.

References

Bellouin, N., Rae, J., Jones, A. Johnson, C., Haywood, J., and Boucher, O.: Aerosol forcing in the Climate Model Intercomparison Project (CMIP5) simulations by HadGEM2-ES and the role of ammonium nitrate, J. Geophys. Res., 116, D20206, doi:10.1029/2011JD016074, 2011.

Bond, T. C. and Bergstrom, R. W.: Light absorption by carbonaceous particles: An investigative review, Aerosol Sci. Technol., 40, 27-67, 2006.

Gunthe, S. S., King, S. M., Rose, D., Chen, Q., Roldin, P., Farmer, D. K., Jimenez, J. L., Artaxo, P., Andreae, M. O., Martin, S. T., and Pöschl, U.: Cloud condensation nuclei in pristine tropical rainforest air of Amazonia: size-resolved measurements and modeling of atmospheric aerosol composition and CCN activity, Atmos. Chem. Phys., 9, 7551-7575, doi:10.5194/acp-9-7551-2009, 2009.

Haywood, J. M., Osborne, S. R., Francis, P. N., Keil, A., Formenti, P., Andreae, M. O., and Kaye, P. H.: The mean physical and optical properties of regional haze dominated by biomass burning aerosol measured from the C-130 aircraft during SAFARI 2000, J. Geophys. Res., 108, 8473, doi:10.1029/2002JD002226, 2003.

Mann, G. W., Carslaw, K. S., Spracklen, D. V., Ridley, D. A., Manktelow, P. T., Chipperfield, M. P., Pickering, S. J., and Johnson, C. E.: Description and evaluation of GLOMAP-mode: a modal global aerosol microphysics model for the UKCA composition-climate model, Geosci. Model Dev., 3, 519-551, doi:10.5194/gmd-3-519-2010, 2010.

Matichuk, R. I., Colarco, P. R., Smith, J. A., and Toon, O. B.: Modeling the transport and optical properties of smoke aerosols from African savanna fires during the Southern African Regional Science Initiative campaign (SAFARI 2000), J. Geophys. Res., 112, D08203, doi:10.1029/2006JD007528, 2007.

Matichuk, R. I., Colarco, P. R., Smith, J. A. and Toon, O. B.: Modeling the transport and optical properties of smoke plumes from South American biomass burning, J. Geophys. Res., 113, D07208, doi:10.1029/2007JD009005, 2008.

Petters, M. D. and Kreidenweis, S. M.: A single parameter representation of hygroscopic growth and cloud condensation nucleus activity, Atmos. Chem. Phys., 7, 1961-1971, doi:10.5194/acp-7-1961-2007, 2007.

Reddington, C. L., Spracklen, D. V., Artaxo, P., Ridley, D. A., Rizzo, L. V., and Arana, A.: Analysis of particulate emissions from tropical biomass burning using a global aerosol model and long-term surface observations, Atmos. Chem. Phys., 16, 11083-11106, https://doi.org/10.5194/acp-16-11083-2016, 2016.

Stokes, R. H. and Robinson, R. A.: Interactions in aqueous nonelectrolyte solutions. I. Solute-solvent equilibria, J. Phys. Chem., 70, 2126-2130, 1966.

van der Werf, G. R., Randerson, J. T., Giglio, L., Collatz, G. J., Mu, M., Kasibhatla, P. S., Morton, D. C., DeFries, R. S., Jin, Y., and van Leeuwen, T. T.: Global fire emissions and the contribution of deforestation, savanna, forest, agricultural, and peat fires (1997-2009), Atmos. Chem. Phys., 10, 11707-11735, doi:10.5194/acp-10-11707-2010, 2010.

van der Werf, G. R., Randerson, J. T., Giglio, L., van Leeuwen, T. T., Chen, Y., Rogers, B. M., Mu, M. Q., Van Marle, M. J. E., Morton, D. C., Collatz, G. J., Yokelson, R. J., and Kasibhatla, P. S.: Global fire emissions estimates during 1997-2016, Earth Syst. Sci. Data, 9, 697-720, 2017.